

This is the accepted manuscript version of the contribution published as:

Sühholz, S., Kopinke, F.-D., Mackenzie, K. (2020):
Reagent or catalyst? – FeS as activator for persulfate in water
Chem. Eng. J. **387**, art. 123804

The publisher's version is available at:

<http://dx.doi.org/10.1016/j.cej.2019.123804>

Reagent or catalyst? - FeS as activator for persulfate in water

Sarah Sühnholz, Frank-Dieter Kopinke and Katrin Mackenzie*

Helmholtz-Center for Environmental Research - UFZ, Department of Environmental Engineering, Permoserstr. 15, D-04318 Leipzig, Germany

Corresponding Author

*Email: sarah.suehnholz@ufz.de. Phone: +493412351584

Abstract

FeS was evaluated as heterogeneous activator for peroxydisulfate (PS) with trichloroethene (TCE) chosen as model substance representing organic water pollutants prone to fast oxidation by sulfate radicals. The TCE degradation followed in most cases pseudo-first-order kinetics with a FeS-normalized maximum rate constant of $k'_{\text{TCE}} = 140 \text{ M}^{-1} \text{ min}^{-1}$ (with $c_{\text{FeS},0} = 0.28 \text{ mM}$ and $c_{\text{PS},0} = 5 \text{ mM}$).

Sulfate radicals were determined as predominant radical species formed during PS activation by FeS by evaluation of the kinetic isotope effect for oxidation of cyclohexanes C_6H_{12} vs. C_6D_{12} ($k_{\text{C}_6\text{H}_{12}} : k_{\text{C}_6\text{D}_{12}} = 2.22$). Monitoring of sulfur and iron species during the course of the reaction revealed that sulfide is rapidly oxidized, whereas $\text{Fe(II)}_{\text{solid}}$ is rather stable over time.

The present study describes in detail the influence of the pH value on the reaction and the long-term performance of FeS as activator for PS with an optimum pH value of 5. On the basis of the radical yield from PS of 1.6 mols $\text{SO}_4^{\bullet-}$ per mol $\text{S}_2\text{O}_8^{2-}$ and the activation energy of

$E_A = (31 \pm 1) \text{ kJ mol}^{-1}$ for the heterogeneous radical generation, a surface-assisted homolytic bond cleavage without simultaneous electron transfer is proposed as activation mechanism, which is contrary to the currently prevailing opinion.

KEYWORDS: persulfate activation – sulfate radicals – iron sulfide – TCE oxidation

1 Introduction

Advanced oxidation processes (AOPs) which are based on sulfate radicals ($\text{SO}_4^{\cdot-}$) have recently gained increasing attention and expand the family of AOP technologies, which were originally based on a number of processes generating hydroxyl radicals (OH^{\cdot}) [1]. Peroxydisulfate (PS, $\text{S}_2\text{O}_8^{2-}$) is a precursor of sulfate radicals, which can also be used for the degradation of persistent pollutants in water [2]. Compared to hydroxyl radicals, sulfate radicals are similarly strong oxidants (standard electrode potential for $\text{OH}^{\cdot}/\text{H}_2\text{O}$ about 2.73 V and for $\text{SO}_4^{\cdot-}/\text{SO}_4^{2-}$ about 2.44 V) [3], but the two radicals differ largely in their reaction pattern. In addition to hydrogen abstraction, which both radicals are able to perform, hydroxyl radicals attach to double bonds, whereas sulfate radicals prefer one-electron transfer reactions. This enables them to facilitate the degradation of recalcitrant compounds which are resistant towards hydroxyl radicals [4]. PS is easy to handle, showing high stability in the solid state and in aqueous solution when activators are absent. There are various ways of PS activation leading to the generation of sulfate radicals and hydroxyl radicals as secondary radicals propagating from sulfate radical reactions [5]. The most effective and common activation methods are UV radiation and heating.

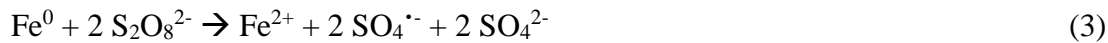
Depending on the pH value, sulfate radicals can react further to hydroxyl radicals according to eqs. (1) and (2) [6]:





By means of chemical probe methods and electron spin resonance spectroscopy, it was shown that PS activation methods in acidic milieu generate predominantly sulfate radicals, whereas at pH values above 9 hydroxyl radicals dominate. Between pH 7 and 9 both radical species are present [7-10]. We do not follow these generalized statements. Rather, the relative reaction rates of sulfate radicals with competing substrates, OH⁻ or organic molecules ($r_{\text{SO}_4^{\cdot-}} = k_i \cdot c_i \cdot c_{\text{SO}_4^{\cdot-}}$), have to be considered. This means, sulfate radicals would dominate the oxidation of benzene ($c_{\text{benzene}} \geq 1 \mu\text{M}$) even at slightly alkaline conditions (pH = 9).

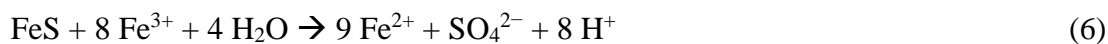
Further methods of PS activation are based on microwave irradiation or the presence of transition metals, carbon materials or alkaline activation [5, 11-17]. In particular, transition metal oxides such as Co₃O₄ and CuO/Fe₃O₄ are receiving increasing attention, because they are easier to handle and more energy-efficient than activation with UV radiation or heat [18-21]. However, cobalt and copper ions leach out under acidic conditions and can cause environmental damage [22-24]. Therefore, environmentally compatible iron species such as zero-valent iron (ZVI), dissolved Fe²⁺ and iron minerals are preferred for PS activation [24-31]. The reactions take place according to the following equations (eqs. 3 - 4) [5, 32]:



The sulfate radicals formed can be quenched by Fe²⁺ forming sulfate ions (eq. 5). Due to its high rate constant (k_3), Fe²⁺ can become a serious competitor to any pollutant to be degraded [33].



In order to maintain low Fe^{2+} concentrations, it is possible to use sulfide-modified ZVI or the poorly water-soluble iron sulfide as source of dissolved Fe^{2+} [34]. Most studies on FeS for water treatment apply it because of its reducing properties for reductive dechlorination of chlorinated compounds such as trichloroethene (TCE) and for reduction of heavy metals such as dichromate [35-44]. To date, there are only very few studies on FeS which show also its abilities to activate PS. The resulting sulfate radicals were used for pollutant decomposition, e.g. 2,4-dinitrotoluene and p-chloroaniline [33, 45-47]. Yuan et al.[33] and Oh et al.[45] state that FeS is a slowly leaching Fe^{2+} source which initiates sulfate radical formation by homogenous reaction according to eq. (4). The activation of PS occurs under neutral and basic conditions with almost unabated rates. In our opinion, there is no clear evidence for the assumption of a purely homogeneous activation mechanism. In recent publications about FeS as PS activator, a heterogeneous activation reaction with radical formation at the FeS surface and subsequent radical diffusion into the aqueous phase is discussed [46]. Furthermore, it was found that Fe^{3+} is reduced to Fe^{2+} by sulfide according to eq. (6).



This reaction occurs stepwise with formation of sulfur intermediates, such as S^0 . In addition, Fan et al.[46] and Chen et al.[47] re-used FeS for PS activation in multiple cycles, but with increasingly lower degradation efficiency. Compiling the data found in the literature on the topic, FeS displays a great potential for PS activation in the context of oxidative water purification, but so far FeS has only been regarded as Fe^{2+} source and not as real catalyst.

The objectives of this study were a deeper understanding of the mechanisms of PS activation by FeS, with the aim of finding the most suitable conditions for pollutant degradation and examining the hypothesis of a catalytic activity of FeS. Until now the studies about FeS as

activator just focused on electron transfer as activation mechanism, which would not explain any catalytic properties of FeS. The effects of pH, FeS and PS concentrations as well as the long-term behavior of the system were studied using the oxidation of TCE as probe reaction. The mechanism of TCE degradation was not part of this study and can be found elsewhere [25].

2 Materials and Methods

2.1 Chemicals

TCE (99.5%) was purchased from Sigma Aldrich. $\text{Na}_2\text{S}_2\text{O}_8$ (PS >99%) was obtained from Roth and Na_2S (59-65%, remainder water) from Honeywell. Na_2SO_4 (anhydrous, p.a.), benzene (GC grade), phenol (p.a.), cyclohexane (99.995%), toluene (Suprasolv), diethyl ether (p.a.), methanol (HPLC grade), chloroform (GC grade), $\text{FeSO}_4 \cdot 7 \text{H}_2\text{O}$ (p.a.), NaOH, 1,10-phenanthroline-monohydrate (p.a.) and H_2O_2 (30%) were all purchased from Merck. 2,4-Dinitrophenylhydrazine (DNPH) and FeS (technical grade, $d_{50} = 20 \mu\text{m}$, $SSA_{\text{BET}} = 0.9 \text{ m}^2\text{g}^{-1}$) were received from Fluka. Phenole- d_6 and cyclohexane- d_{12} (99.6%) were obtained from Aldrich. KI (>99%) was received from J.T.Baker. HCl (35-38%), formaldehyde (37%) and isopropanol (99.95%) were purchased from Chemsolute.

2.2 Dechlorination experiments

TCE (7.5 mM) and PS (197 mM) stock solutions were prepared with deionized water. For the experiments under uncontrolled pH conditions (starting pH = 7), the reactions were carried out in 60 mL crimped serum bottles. A defined amount of FeS and 0.8 mL of TCE stock solution were added to 40 mL of a 10 mM Na_2SO_4 solution ($c_{0,\text{TCE}} = 0.15 \text{ mM}$). The gas phase was sampled and analyzed using a GC-MS device. The addition of 1.2 mL of PS stock solution to the bottles

marked the reaction start (t_0). For steady mixing of the suspension, the bottles were shaken at room temperature on a horizontal shaker at 250 rpm. Periodically, the gas phase was analyzed with GC-MS directly. 1 mL aqueous samples (maximum 10% of the total volume) were collected from the bottles for analysis of PS, chloride and dissolved iron concentrations. These experiments were carried out under O₂ or N₂ atmosphere and with H₂O₂ addition where stated. Furthermore, blind experiments without either FeS or PS were performed in order to determine the contribution of these two compounds to TCE degradation.

For pH-controlled reactions, the experiments were conducted in 250 mL flasks with two ports in 166 mL with the same concentrations mentioned above. In order to maintain a constant pH value, sodium hydroxide solution (0.01 M) was added by means of a titroline alpha plus (Schott Instruments, Germany). In order to ensure that no TCE was lost during the experiment, a reactor was used where the ports were equipped with the electrode and the dosing element through PTFE-lined silicon septa providing gas-tight connection. Furthermore, blank experiments were performed in order to judge any possible loss of TCE during the reaction time. In addition, Ar was used as internal headspace standard.

2.3 Mechanistic studies

Experiments without TCE were carried out in parallel batches in 30 mL flasks with 5 mM FeS (suspended) and 11 mM PS in 20 mL of 10 mM Na₂SO₄ solution at different pH values (3, 5, 7 and 9). After 10 min, 30 min, 60 min, 120 min, 240 min and 24 h, one of the flasks was centrifuged in order to separate the solid from the liquid phase. From each of the batches the aqueous phase was analyzed the dissolved iron and remaining PS concentration. The solid phase was characterized by determination of the concentrations of total iron, Fe²⁺ and sulfide.

Kinetic isotope effect (KIE) experiments were carried out in 120 mL crimped serum bottles with 1.2 mM FeS, 2.1 mM PS and 83 μM cyclohexane-d₀ and -d₁₂ each in 118 mL distilled water with a starting pH = 7. In order to minimize the gas fraction of the cyclohexane isotopologues, the headspace volume was kept small (2 mL). The reaction progress was followed over time by GC-MS analysis of gas samples from the headspace.

In order to determine the effect of the shaking intensity (5 and 560 rpm), the experiments were carried out in 120 mL crimped serum bottles with 2 mM FeS, 2.5 mM PS and 80 μM cyclohexane in 118 mL distilled water with a starting pH = 7. When working with the very volatile cyclohexane, the headspace volume was kept small (2 mL) to minimize its gas fraction during reaction. The reaction progress was followed over time by GC-MS analysis of gas samples from the headspace.

In order to test the catalytic nature of the PS activation by FeS, the batch experiment was prepared as described above at different pH values, whereby isopropanol was added as radical scavenger. Small amounts of FeS (10-30 μmol in 100 mL water) were used and the initial PS

concentration was adjusted to at least 90 times higher than the FeS concentration. The PS concentration was measured frequently.

The yield of sulfate radicals was determined with 4 M methanol and 0.17 mM PS in 30 mL. The PS was activated by FeS (4.6 mM), FeSO₄ (3.6 mM), heat (60°C) or UV (254 nm) with a starting pH = 7. The primary oxidation product of methanol (formaldehyde) was derivatized with DNPH and analyzed by means of HPLC-UV.

For determination of the activation energy of the PS decomposition, 50 mL of a 13 mM aqueous benzene solution were used. PS (5 mM) was activated by particulate FeS (2.3 mM) or by dissolved FeSO₄ (0.7 mM) at various temperatures (273, 283 and 298 K) with a starting pH = 7. All solutions were initially adjusted to the respective temperature before mixing. Frequently, 0.5 mL of the aqueous phase were removed, mixed with a NaOH solution in order to stop the reaction and extracted with 3 mL chloroform. The extracts were analyzed by means of GC-MS for phenol. The quantification was performed using toluene as internal standard.

2.4 Chemical analysis

Chloride analysis was performed by means of an ion chromatograph (IC 25, Dionex equipped with an IonPacAS15/AG15 column). TCE, cyclohexane, benzene, phenol, sulfide and polysulfides (as H₂S_n after acidification) were determined during the batch experiments using a GC-MS-QP2010 (Shimadzu, equipped with a HP5 capillary column, carrier gas was helium). Formaldehyde was measured as DNPH-derivative with HPLC-UV (HPLC Series 1100 from Hewlett Packard, equipped with a Kinetex 2.6 μm XB-C18 100 Å, LC column). Concentrations of total dissolved iron were determined using spectroquant iron tests (Merck) and an UV-Vis spectrophotometer (photolab 6600 UV-VIS series, WTW, Germany). The persulfate

concentrations were determined using the spectrophotometric method, measuring the absorbance of I_3^- at 352 nm according to [48]. In order to identify the total iron and Fe^{2+} concentrations in the solids, they were separated after centrifugation from the liquid phase and then dissolved in concentrated HCl. Total iron concentrations were determined as described above and Fe^{2+} was characterized using 1,10-phenanthroline as complexing agent by UV-Vis spectrophotometric analysis. The samples were handled under exclusion of air. The H_2S formed during the dissolution of the solid residue in HCl was purged and oxidized to SO_4^{2-} with H_2O_2 under alkaline conditions and measured by means of ion chromatography.

3 Results and Discussion

3.1 Peroxydisulfate activation by FeS

In accordance with previous reports in the literature, reactions of PS with dissolved ferrous ions are fast in the first minutes, whereas after this initial period, the degradation of TCE stagnated due to consumption of Fe^{2+} by sulfate radicals (see eq. 5). For an efficient pollutant removal, it is necessary to add Fe^{2+} successively in small amounts [49]. In comparison to dissolved ferrous ions, FeS ($c_{PS,0} = 6$ mM, $c_{FeS,0} = 3$ mM) achieved, as activator of the persulfates, nearly complete removal of TCE within 20 min (see Fig. 1).

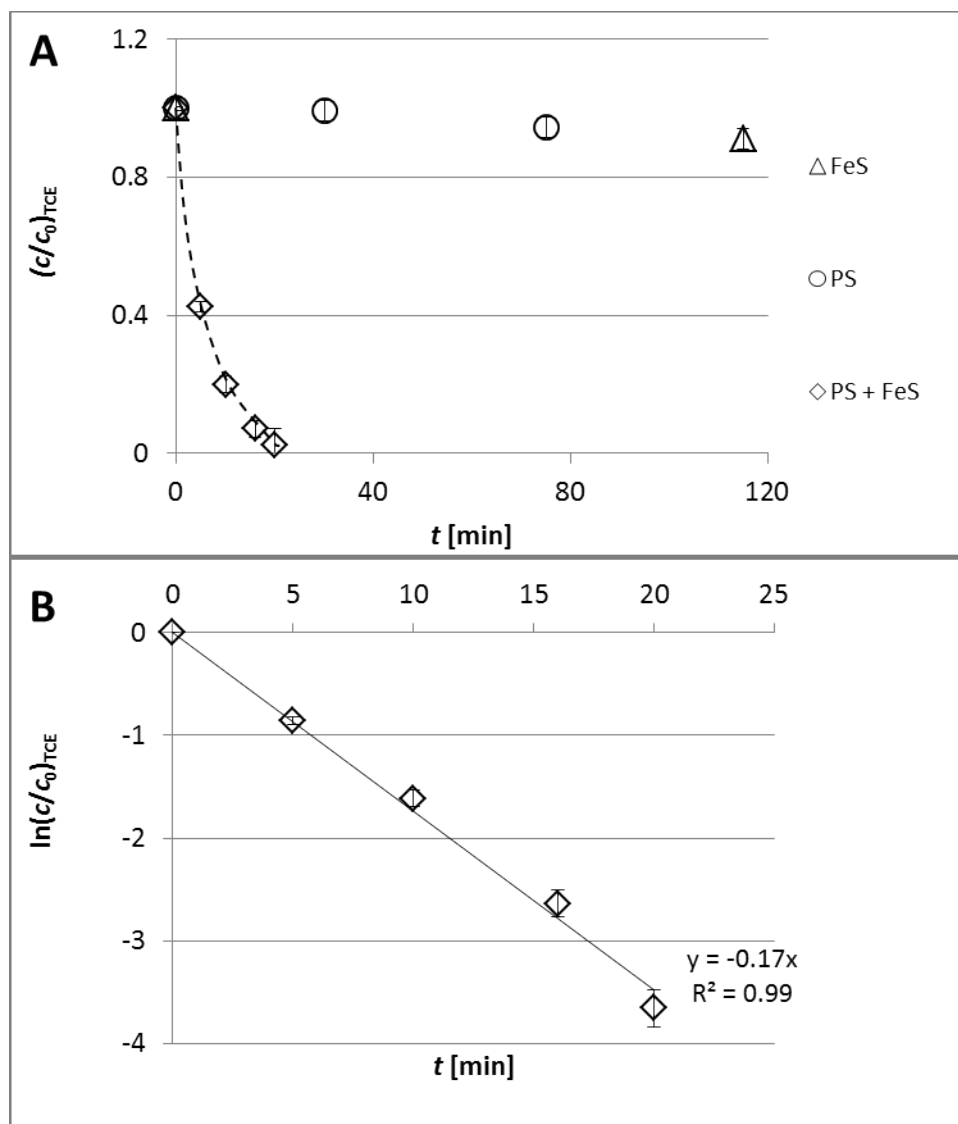


Figure 1: Decrease in TCE concentration during the oxidation by peroxydisulfate activated with FeS (A) and first-order kinetics of TCE degradation (B) ($c_{0,TCE} = 150 \mu\text{M}$, $c_{PS,0} = 6 \text{ mM}$, $c_{FeS,0} = 3 \text{ mM}$, pH 3). Error bars show one standard deviation of single analyses from the mean value.

As there is only a slow reaction under the chosen conditions between TCE and PS, as well as between TCE and FeS alone, FeS is identified as an activator for PS. The degradation of TCE in the system can approximately be described by pseudo-first-order reaction kinetics according to eq. (7).

$$c_{t,\text{TCE}} = c_{0,\text{TCE}} \cdot e^{-k_{\text{obs}} \cdot t} \quad (7)$$

The observed reaction rate constant for TCE degradation was found to be $k_{\text{obs}} = 0.17 \text{ min}^{-1}$ for PS as sulfate radical source with activation by FeS. As the rate constant for TCE attack by sulfate radicals is rather high ($k_{\text{SO}_4^{\bullet-} + \text{TCE}} \approx 10^9 \text{ M}^{-1} \text{ s}^{-1}$) [50] one can assume that the rate limiting step in the FeS-mediated oxidation of TCE is the PS activation (see Fig. S1).

Shaking intensity affects observable reaction rates (see Fig. S2); this clearly indicates the heterogeneous nature of the reaction. However, it should be mentioned that the chosen conditions were always in the plateau of observable rates, which means that even at faster shaking, the reaction rate does not change.

3.2 Investigation of radical species

Hydroxyl and sulfate radicals can be distinguished by means of their reaction selectivities. One measure is the H-KIE of a hydrogen abstraction reaction [51]. For $\text{KIE} = k_{\text{H}}/k_{\text{D}} \approx 1.1$, hydroxyl radicals are the predominant species [52]. Sulfate radicals are expected to affect significantly larger H-KIEs ≥ 2 . In this study, FeS was used as an activator of PS, and the prevailing radicals were revealed by means of oxidation of a mixture of the cyclohexane isotopologues (C_6H_{12} and C_6D_{12}). Activation of PS results in $\text{H-KIE} = k_{\text{C}_6\text{H}_{12}}/k_{\text{C}_6\text{D}_{12}} = 2.22 \pm 0.03$ (Fig. 2), indicating sulfate radicals as the predominant attacking radicals. Other studies have shown that hydroxyl radicals can also play a role in the degradation of pollutants. These radicals are probably emerging from the reaction of $\text{SO}_4^{\bullet-}$ with water or hydroxide ions according to eqs. (1) and (2) [46, 47]. The different observations made in this study can be explained by the fact that sulfate radicals react much faster with cyclohexane than with water ($k_{\text{SO}_4^{\bullet-} + \text{C}_6\text{H}_{12}} = 4 \cdot 10^8 \text{ M}^{-1} \text{ s}^{-1}$) [6]. The comparison of relative reaction rates ($r_{\text{C}_6\text{H}_{12}}/r_{\text{H}_2\text{O}} = 4 \cdot 10^8 \text{ M}^{-1} \text{ s}^{-1} \cdot 83 \mu\text{M} / (3 \cdot 10^3 \text{ s}^{-1}) \approx$

10) yields a factor of ≥ 10 in favor of H-abstraction from cyclohexanes rather than from water under the applied conditions.

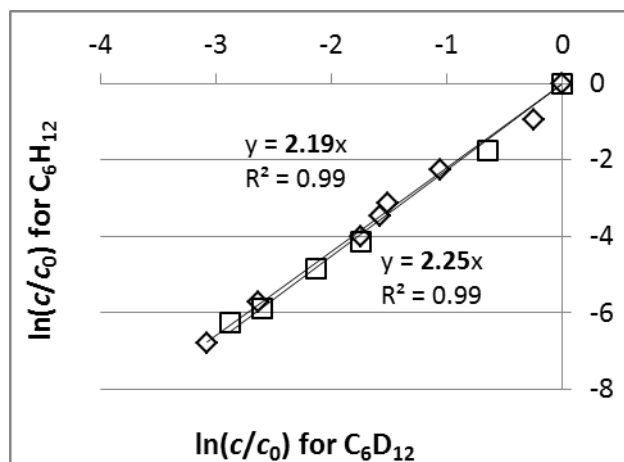


Figure 2: Determination of the kinetic isotope effect for oxidation of cyclohexane-d₀ and -d₁₂ with PS activated by FeS ($c_{0,\text{cyclohexanes}} = 83 \mu\text{M}$ each, $c_{0,\text{FeS}} = 1.2 \text{ mM}$, $c_{0,\text{PS}} = 2.1 \text{ mM}$, initial pH = 7). The different symbols represent two independent experiments.

3.3 Influence of reaction conditions on TCE degradation kinetics

Table 1 shows observed pseudo-first-order rate constants for the TCE degradation at various initial TCE, PS and FeS concentrations. For $c_{\text{TCE}} \leq 150 \mu\text{M}$ the degradation reaction follows pseudo-first-order kinetics with a reaction rate constant of approximately $k_{\text{TCE}} = 0.3 \text{ min}^{-1}$ ($c_{0,\text{PS}} = 5 \text{ mM}$, $c_{0,\text{FeS}} = 2.8 \text{ mM}$). At $c_{0,\text{TCE}} = 750 \mu\text{M}$, the reaction kinetics follows a pseudo-zeroth-order over the main concentration range, but was roughly approximated by a pseudo-first order constant $k_{\text{TCE}} \approx 0.13 \text{ min}^{-1}$. At initial FeS concentrations of 0.28, 2.8, 5.7 and 27 mM, increasing reaction rate constants of $k_{\text{TCE}} = 0.04, 0.30, 0.65$ and 0.95 min^{-1} , respectively, were measured. Up to 5.7 mM, the TCE oxidation rate was proportional to the initial FeS concentration, yielding FeS-normalized second-order rate constants of $k'_{\text{TCE}} = (120 \pm 20) \text{ M}^{-1}\text{min}^{-1}$. This finding indicates that FeS is directly involved in the rate-controlling step. Only at high FeS

concentrations (27 mM) the second-order rate constant decreases. It is described in the literature that for Fe-based activators, the increase in reaction rates with increasing activator concentration is limited due to quenching of sulfate radicals (eq. 5) [10, 53-55]. Increasing PS concentrations also effect higher TCE oxidation rates of up to about 5 mM. For higher PS concentrations, no further increase in the TCE reaction rates was observed. The nature of the underlying radical quenching processes remains unidentified. Thus, it can be concluded that there is an optimal set of reaction conditions, where a maximal steady state concentration of sulfate radicals is available for substrate oxidation, as has also been observed in other studies [33, 56]. In the present study, the most effective concentrations are about 5 mM for FeS and PS (or slightly higher). The window of optimal concentrations is also affected by the FeS specific surface area. This result is in good agreement with the literature [33]. The pseudo-first-order reaction rate constants observed in this study are remarkably high compared to those reported for other iron-based activators. Magnetite as activator showed an observed reaction rate constant of 0.015 min^{-1} (5 g L^{-1} magnetite, 252 mM PS, 0.15 mM TCE) [56]. Iron salts with various chelating agents reached reaction rate constants of about 0.12 min^{-1} (10 mM Fe(II)-EDTA, 2 μM TCE, 0.5 mM PS) [57] and 0.09 min^{-1} (0.3 mM Fe^{2+} , 2.25 mM PS, 0.15 mM citric acid, 0.15 mM TCE) [58]. A more suitable basis for comparison of kinetic data is the second-order rate constant normalized to the introduced iron equivalent. Using the above data, we calculate values of $0.23 \text{ M}^{-1}\text{min}^{-1}$ for magnetite, $12 \text{ M}^{-1}\text{min}^{-1}$ for $\text{Fe}^{2+}\text{edta}$, $300 \text{ M}^{-1}\text{min}^{-1}$ for Fe^{2+} with citric acid as chelating agent, and $120 \text{ M}^{-1}\text{min}^{-1}$ for FeS ($c_{0,\text{PS}} = 5 \text{ mM}$, $c_{0,\text{FeS}} = 5.7 \text{ mM}$, this study). Heat activation of PS reached a reaction rate constant k_{TCE} of approximately 0.05 min^{-1} at $70 \text{ }^\circ\text{C}$ and $c_{0,\text{TCE}} = 2 \text{ mM}$, $c_{0,\text{PS}} = 20 \text{ mM}$ [11]. This comparison shows that FeS is an effective activator for PS, allowing high reaction rates for TCE degradation.

Table 1 compiles reaction rate constants for TCE oxidation in the FeS/PS system under various reaction conditions. Experiments 4, 5 and 9 with high ratios of TCE to FeS or PS concentrations show the same tendency: the observed TCE concentration vs. time curves follow more a zeroth- than first-order kinetics. This is consistent with a high yield of radical consumption by TCE, where the radical formation is the rate-limiting step. Furthermore it can be seen that at higher PS and FeS concentrations the reaction does not proceed faster because of increased radical consumption by PS itself and Fe^{2+} released into the water bulk phase. They then start to compete with TCE for sulfate radicals at eye level. This observation for TCE has considerable relevance for the transferability to degradation of other pollutants with similar reactivity towards sulfate radicals and for the use of this method in water purification [33].

Table 1: Kinetic parameters of TCE degradation with variation of reactant concentrations.

Exp. no.	Initial concentrations	Pseudo-first-order rate constant, k_{TCE} (min^{-1})	Pseudo-zeroth-order rate constant, k^*_{TCE} ($\mu\text{M min}^{-1}$)	Iron-normalized second-order rate constant, k'_{TCE} ($\text{M}^{-1} \text{min}^{-1}$) $= k_{\text{TCE}}/c_{0,\text{FeS}}$
$c_{0,\text{PS}} = 5 \text{ mM}$, $c_{0,\text{FeS}} = 2.8 \text{ mM}$				
1	TCE = 27 μM	$0.32 \pm 0.06^{**}$		112
2	TCE = 75 μM	0.30 ± 0.07		105
3	TCE = 150 μM	0.32 ± 0.02		112

4*	TCE = 750 μ M	0.132 ± 0.001	14.1 ± 0.8	46
$c_{0,TCE} = 75 \mu\text{M}, c_{0,PS} = 5 \text{ mM}$				
5*	FeS = 0.28 mM	0.040 ± 0.004	1.41 ± 0.03	140
6	FeS = 2.8 mM	0.30 ± 0.07		105
7	FeS = 5.7 mM	0.65 ± 0.07		114
8	FeS = 27 mM	0.95 ± 0.02		34
$c_{0,TCE} = 75 \mu\text{M}, c_{0,FeS} = 2.8 \text{ mM}$				
9*	PS = 0.1 mM	0.045 ± 0.007	2.4 ± 0.7	16
10	PS = 1 mM	0.10 ± 0.01		35
11	PS = 5 mM	0.30 ± 0.07		105
12	PS = 10 mM	0.27 ± 0.02		95

* Pseudo-zeroth-order. **The indicated intervals are one standard deviation of single values from the mean value from 3 replicates.

3.4 Effect of pH and oxygen content on TCE degradation

Experiments concerning the effect of the pH value and the presence of oxygen during the degradation of TCE were carried out at four different pH values (3, 5, 7, 9) kept constant during the entire reaction time and in three different scenarios: (i) without gas purging, i.e. in the presence of air, (ii) purging with N₂ and (iii) addition of H₂O₂ without purging. As the literature

mentioned FeS as a source for Fe^{2+} experiments with H_2O_2 were carried out to see if there is a synergistic effect between iron and H_2O_2 as in the Fenton reaction. Figure 3A-D show that the rate of TCE degradation follows the trend $\text{pH } 5 > \text{pH } 3 > \text{pH } 7 > \text{pH } 9$.

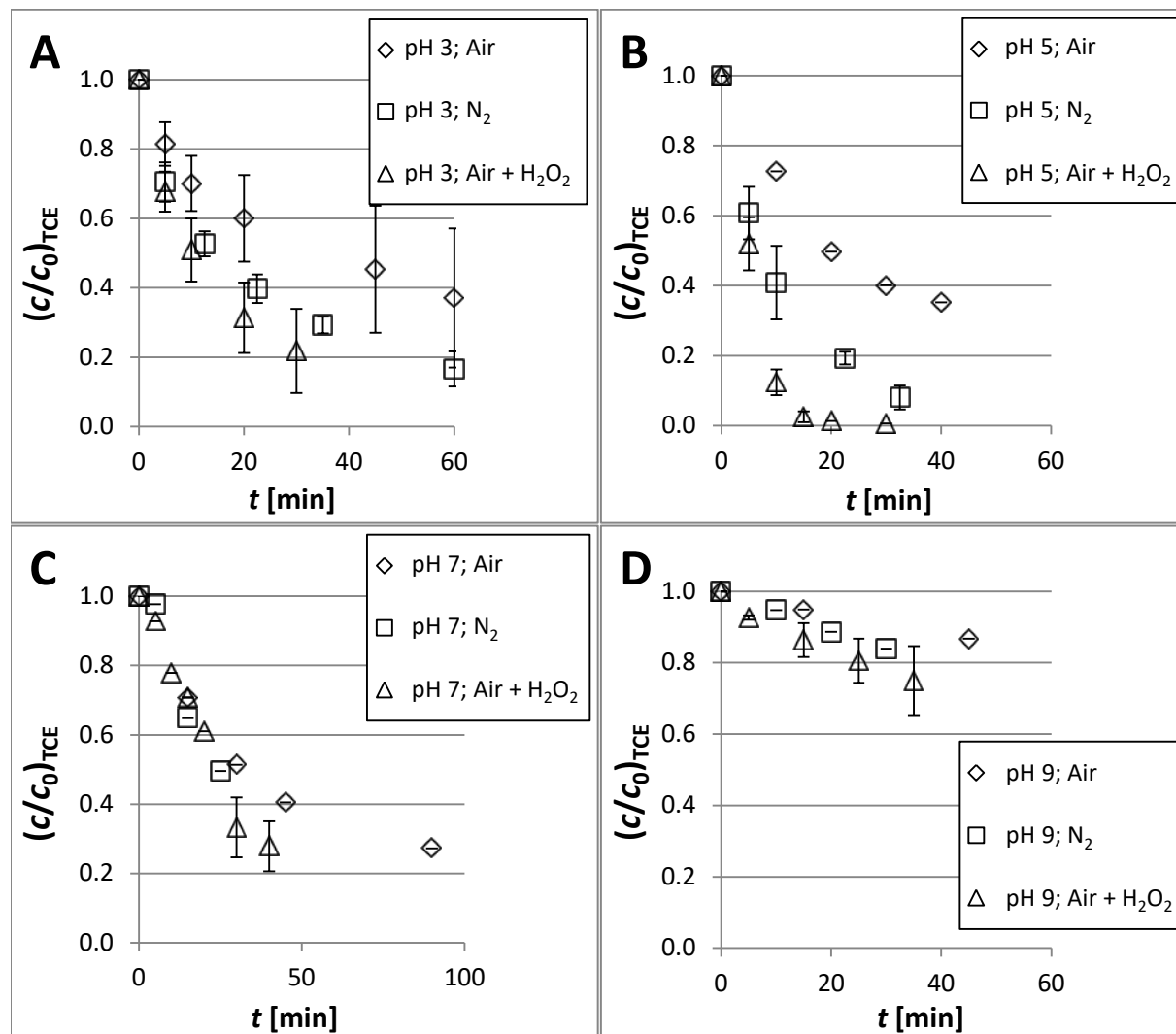


Figure 3: TCE oxidation by persulfate activated with FeS ($c_{0,\text{TCE}} = 0.15 \text{ mM}$, $c_{0,\text{PS}} = 6.3 \text{ mM}$, $c_{0,\text{FeS}} = 569 \text{ }\mu\text{M}$, $c_{\text{Na}_2\text{SO}_4} = 10 \text{ mM}$, $c_{0,\text{H}_2\text{O}_2} = 0.1 \text{ }\mu\text{M}$) under various conditions.

For p-chloroaniline degradation, different results for optimum pH conditions are described in the literature. Yuan et al.[33] found that a starting pH of 7 results in the highest reaction rate,

whereas Fan et al.[46] stated, in accordance with the present study, that the reaction has its optimum at pH = 5. The slower reaction under alkaline conditions (Fig. 3D) can be explained by the formation of iron hydroxide at the surface of FeS as well as a negative surface charge at higher pH values and thereby an electrostatic repulsion of the persulfate ion [59]. Due to the so-formed oxidic surface layer, the activation of PS is probably inhibited. Even under neutral conditions the formation of such an oxide shell is likely.

It is noticeable that TCE degradation is more efficient at pH 5 (Fig. 3B) than at pH 3 (Fig. 3A). At the lower pH value, PS activation by FeS is increasingly superimposed by homogenous PS activation by dissolved Fe²⁺ (see eq. 5). The latter seems to occur with lower reaction rates than with heterogeneous activation by FeS. This result agrees with the observations made by Fan et al. [46]. Another explanation for the slower reaction at lower pH values is the acid catalyzed side reaction of persulfate, where the persulfate reacts over a sulfur tetroxide to oxygen and sulfur trioxide and further to sulfuric acid [60].

For all pH conditions, the reaction rate (compiled in Table 2) follows the trend that non-purged systems with additional H₂O₂ allow a higher TCE degradation rate, followed by oxygen-free systems (purged with N₂). The unpurged batch experiments (in presence of air) without H₂O₂ showed the lowest reaction rates. These results differ from observations made in previous studies using FeS₂, where dissolved oxygen promotes the degradation of organic pollutants. Zhang et al.[61] and Xia et al.[62] suspected that oxygen reacts with Fe(II)_{solid}-species (solid ferric iron on the surface of the material) to superoxide radicals, which are also able to activate PS (see eqs. 8 and 9).



The different behavior of FeS and FeS₂ can possibly be explained by different crystal structures. Fe(II) in FeS might react with oxygen to an iron-oxide surface layer, whereas the Fe(II) in FeS₂ could lead to the formation of superoxide radicals in addition to iron oxide formation [63]. In the present study, this results in a lower reaction rate in the presence of dissolved oxygen. The significantly faster degradation of TCE in the case of H₂O₂ addition is not due to direct reaction with TCE (see Fig. S3) but might be related to the re-reduction of Fe³⁺ to Fe²⁺ with H₂O₂ and therefore support the catalytic cycle as is known from the Fenton reaction [64]. In addition, H₂O₂ itself is a source of OH-radicals which can contribute to the TCE oxidation. This reaction is an exothermic reaction where the heat release in more concentrated solutions can influence the reaction kinetics [65]. In order to gain further insight and to evaluate the established hypotheses, the activation mechanism of PS with FeS was investigated.

Table 2: Reaction rate constants k_{obs} [min⁻¹] for TCE oxidation by FeS-activated PS at various pH values.*

pH	air	purging with N ₂	air + H ₂ O ₂
3	0.02 ± 0.01	0.030 ± 0.005	0.05 ± 0.02
5	0.03 ± 0.01	0.08 ± 0.01	0.23 ± 0.02
7	0.02 ± 0.01	0.03 ± 0.01	0.03 ± 0.01
9	0.003 ± 0.001	0.006 ± 0.001	0.009 ± 0.003

* Evaluation according to pseudo-first-order reaction kinetics. The indicated variations are one standard deviation from the mean value from two replicates each.

3.5 Mechanistic investigations

3.5.1 Influence of reaction conditions on the PS/FeS system

In this section, the influences of the pH value and the atmospheric conditions (oxygen, oxygen-free and oxygen plus H₂O₂) on the FeS particles are discussed. Figure 4A-F shows the relative concentrations of dissolved iron and Fe²⁺ in the solid.

It can be seen that at pH 3 the highest proportion of iron is present in the dissolved state under all atmospheric conditions (Fig. 4A-C). Between pH 5 and 7, there is almost no iron in solution; under alkaline conditions, only a low percentage of iron is dissolved, which can be associated with the formation of hydroxo complexes [66]. In other studies with FeS as activator for PS, the dissolved iron contents measured are inconsistent. Yuan et al.[33] and Chen et al.[47] calculated that at pH 3, about 20% of the total iron was available in solution and that 10% iron oxide was formed after 4 h, which is in conformity with the results of this study. Contradicting, Fan et al. [46] detected the complete dissolution of iron as Fe²⁺ at pH 3.

The iron remaining in the solid phase is gradually oxidized from Fe²⁺ to Fe³⁺ for all pH values except pH 9 in the presence of dissolved air (Fig. 4D). The lowest Fe²⁺ content at the end of the experiment after 24 h was found at pH 7. At pH 3 and 5, Fe²⁺ is more stable and the oxidation proceeds slower. One might expect that at pH 9, Fe²⁺ would be less stable than in more acidic milieus, thus it was suspected that the Fe²⁺ content would be lowest at that pH [67]. However, the observations made in this study did not confirm this hypothesis. A possible explanation is the formation of protective layers, possibly consisting of Fe²⁺-hydroxo complexes. When oxygen is excluded, this effect is not observed and at pH 9, more Fe²⁺ is oxidized than at pH 3 and 5 (Fig. 4E).

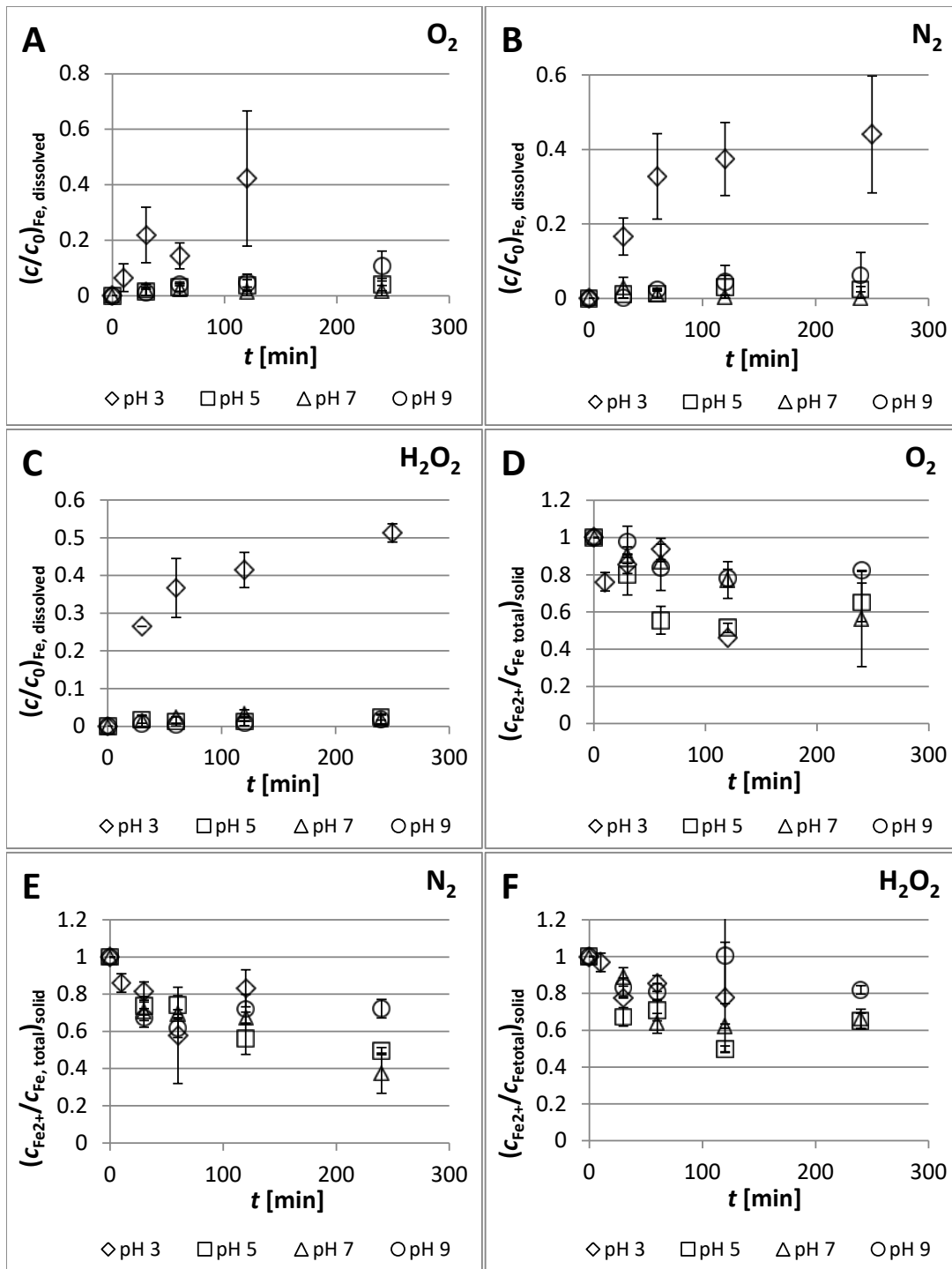


Figure 4: Effects of the pH value on the dissolved iron share of total iron over time in the presence of air (A), N₂ (B) or air and H₂O₂ (C) as well as the Fe²⁺ content in the solid phase over time in the presence of air (D), N₂ (E) or air and H₂O₂ (F) ($c_{\text{PS},0} = 14.3$ mM, $c_{\text{FeS},0} = 4.55$ mM, $c_{\text{Na}_2\text{SO}_4} = 10$ mM, $c_{0,\text{H}_2\text{O}_2} = 0.1$ μM).

When H_2O_2 is added, the Fe^{2+} content is much higher during the reaction at all pH values (Fig. 4F). This observation suggests that even catalytic amounts of H_2O_2 promote the reduction of Fe^{3+} to Fe^{2+} . This effect is known from the Fenton reaction [68].

As shown in Figs. S4-6, the decrease in PS concentration was similar in all experiments except for those at pH 5 in the unpurged system, where a significantly slower PS degradation was found. The degradation of PS stagnates after some time at all pH values, presumably due to the lack of radical consumers (Table S1). In summary, it can be stated that lower pH values as well as the H_2O_2 addition lead to an earlier stagnation of PS decomposition.

Sulfide is oxidized rapidly and precipitates as sulfur at all pH values except pH 3, where the ratio of $n_{\text{sulfide}} : n_{\text{Fe}^{2+}}$ remains at about 1 for the oxygen-containing and the oxygen-free system (Fig. S4B). This means that at pH 5, 7 and 9, sulfide is not stable and other Fe(II) species, such as oxides, must be present in the solid grain. We found that in the presence of H_2O_2 , sulfide is immediately oxidized to elemental sulfur, which gave the reaction suspension a milky appearance for a considerable time.

3.5.2 Investigation of the nature of PS activation: stoichiometric or catalytic?

In order to clarify whether FeS acts as a reagent or catalyst in the activation of PS, the PS conversion during multiple activation cycles was investigated at various pH values in the presence of isopropanol as radical quencher. At pH 3, 5 and 7, the approximately 100-fold stoichiometric amount of PS compared to the FeS present was activated (see Fig. 5). Thus, it can be clearly concluded that under these conditions FeS activates PS in a catalytic manner. Fan et al.[46] suggested that sulfide reduces Fe^{3+} to Fe^{2+} , which in turn can repeatedly activate PS. In that case, due to the transfer of 8 electrons during oxidation of sulfide to sulfate, the 9-fold stoichiometric amount of PS could be activated (see eq. 6). However, this 9:1 stoichiometry

cannot explain the observed 100:1 activation ratio. Furthermore, extraction of the reaction mixture at the end of the experiment with CHCl_3 revealed the presence of elemental sulfur, which means that there must be another mechanism affecting the activation of PS. It is noticeable that at pH 3, 5 and 9, the PS decomposition rates slow down after repeated PS doses (Table 3, Figure 5A, B, D). This observation could be explained by the oxidation of iron by radicals or oxygen. At pH 7, the PS degradation rate appears to increase over time. An explanation has not yet been proposed, thus the effect should be further investigated. In some studies it was found that isopropanol can lead to PS consumption with increasing reaction rates. However this consumption occurred either at high pH values or in absence of dissolved oxygen [69, 70]. In presence of oxygen, side reactions were discussed to interfere.

Table 3: First-order rate constants (in h^{-1}) for PS degradation at various pH values. Experimental details according to the legend of Figure 5.

Cycle	pH 3	pH 5	pH 7	pH 9
1	0.12	0.034	0.009	0.003
2	0.11	0.015	0.018	
3	0.10		0.025	
4	0.06			
5	0.03			
6	0.01			

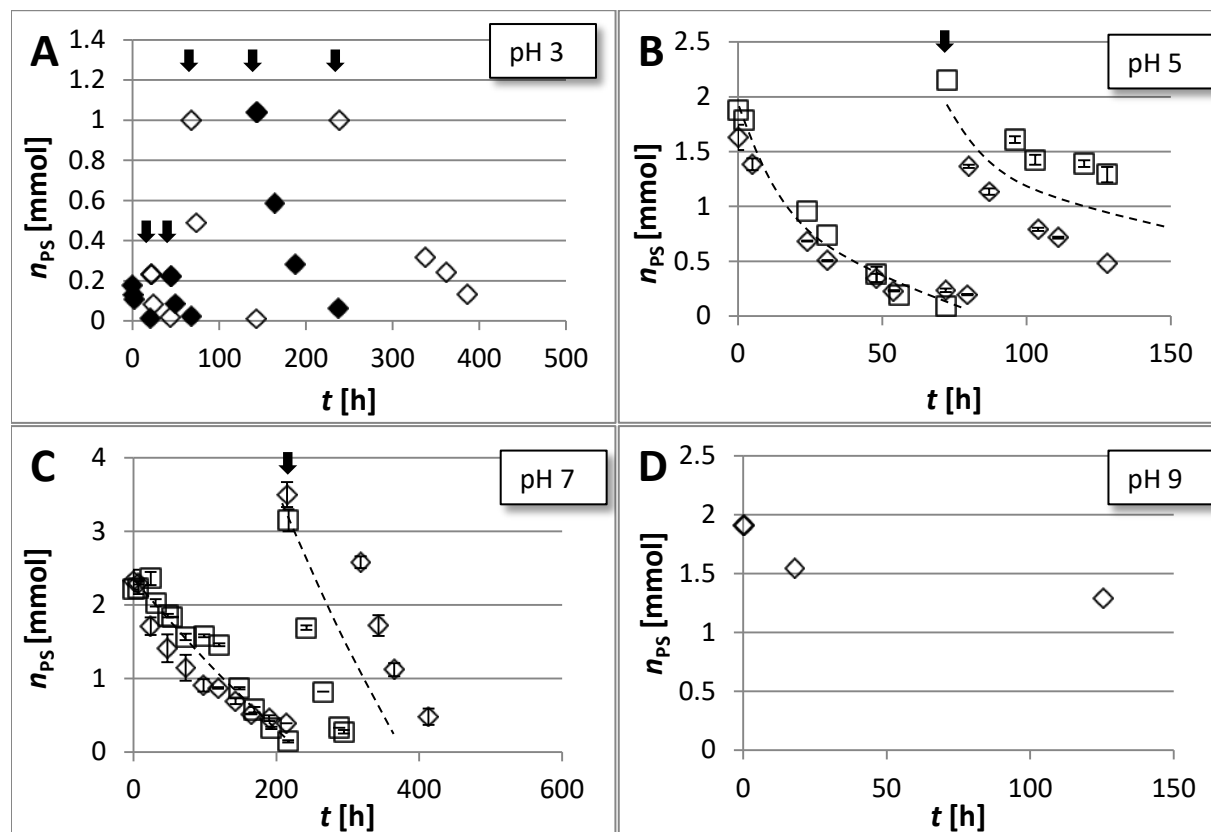


Figure 5: PS decomposition with 20 μmol FeS and 65 mmol isopropanol as radical quencher with multiple PS additions at various pH values. Two symbols represent results of two parallel experiments; arrows symbolize repeated PS addition. Due to pH stabilization and increasing volume (max. 25% for experiments B and C), no concentrations are given here (all amounts in initially 100 mL water). Error bars show multiple measurements of one experiment; the lines were added to guide the eye.

3.5.3 Sulfate radical yield

The yield of sulfate radicals from PS is a key feature of any activation method. It determines the efficiency of PS as radical source and may provide additional information about the reaction mechanism. Methanol was used as target substrate due to the clear reaction mechanism and the

formation of formaldehyde as the sole primary oxidation product ($\text{CH}_3\text{OH} + 2 \text{SO}_4^{\cdot-} \rightarrow \text{CH}_2\text{O} + 2 \text{HSO}_4^-$). Table 4 summarizes the rate constants of the reaction of sulfate radicals with radical-consumers present in the system. As can be seen by the reaction-probability check ($k \cdot c$), sulfate radicals mainly react with methanol and dissolved Fe^{2+} .

Table 4: Second-order rate constants for reactions of compounds present in the investigated system with sulfate radicals [6].

Component	Reaction rate constant k [$\text{M}^{-1} \text{s}^{-1}$]	Concentration c [M]	$k \cdot c$ [s^{-1}]	Relative reaction rates u_i/u_{methanol} [-]
Methanol	$2 \cdot 10^7$	4	$8 \cdot 10^7$	1
Fe^{2+}	$9.9 \cdot 10^8$	$< 4 \cdot 10^{-3}$	$< 4 \cdot 10^6$	< 0.05
H_2O	$6 \cdot 10^1$	55.56	$3 \cdot 10^3$	$3.7 \cdot 10^{-5}$
PS	$1.2 \cdot 10^6$	$0.3 \cdot 10^{-3}$	$0.3 \cdot 10^3$	$3.7 \cdot 10^{-6}$

In Table 5, the resulting formaldehyde yields are shown. The high concentration (4 M) and stoichiometric surplus of methanol ($n_{\text{methanol}} : n_{\text{PS}} = 2.35 \cdot 10^4$) ensure an efficient trapping of the sulfate radicals formed. The measured formaldehyde yield of $(98 \pm 16)\%$ for heat activation of PS is close to the theoretical value of 100% according to $\text{S}_2\text{O}_8^{2-} + \text{heat} \rightarrow 2\text{SO}_4^{\cdot-}$. This supports the validity of the applied method. The formaldehyde yield of $(80 \pm 2)\%$ achieved by FeS activation at ambient temperature was slightly lower, but still significantly above the value of 50% expected from the heterolytic cleavage of PS according to $\text{S}_2\text{O}_8^{2-} + \text{e}^- \rightarrow \text{SO}_4^{\cdot-} + \text{SO}_4^{2-}$ [4, 19]. Higher yields indicate that homolytic bond cleavage – with generation of two sulfate

radicals per decomposed PS molecule – plays the major role for FeS activation. The slightly lower formaldehyde yield with FeS compared to heat activation could be due to additional radical quenchers in the FeS system. In addition, the reaction temperatures are different in the two reaction samples (23°C vs. 60°C). Based on the high sulfate-radical yield, we hypothesize a surface assisted, homolytic cleavage of the O-O-bond in PS. Based on the high sulfate-radical yield, we hypothesize a surface assisted, homolytic cleavage of the O-O-bond in PS. This means persulfate will coordinative bind to surface Fe atoms through donation of O electrons to empty $3d$ Fe orbitals (LUMO, Fe d_z^2) resulting in the formation of Fe–O type surface states. This is already known from other processes [71]. Because of the larger distances between the iron atoms (510 pm) in FeS lattice compared to the O-S-O-O-S-O bond distance (ca. 450 pm), the O-O bond in the peroxy function (ca. 146 pm) is predominantly stretched in the adsorbed state leading to a decrease in the activation energy (see Scheme 1). For the confirmation of the hypothesis, quantum mechanical modeling would be useful. For understanding of the activation mechanism in the FeS/PS system our hypothesis is a remarkable new aspect.

Table 5: Yields of formaldehyde (in mM) from methanol (4 M) oxidation with 0.17 mM PS activated by FeS (4.6 mM), FeSO₄ (3.6 mM), heat (60°C) or UV (254 nm).

Heat + PS	FeS + PS	UV + PS	FeSO ₄ + PS
0.169 ± 0.030	0.13 ± 0.01	0.17	0.07 ± 0.01

UV activation of PS also generates almost 100% formaldehyde yield. The PS activation with dissolved ferrous iron provided the lowest formaldehyde yield (41%), as is to be expected from the reaction stoichiometry.

A high formaldehyde yield from methanol oxidation could also be explained by contributions of radical chain reactions (e.g. $\bullet\text{CH}_2\text{-OH} + \text{S}_2\text{O}_8^{2-} \rightarrow \text{CH}_2=\text{O} + \text{SO}_4^{\bullet-} + \text{HSO}_4^-$) as found by Bartlett and Cotman for elevated temperatures [72]. Such radical chain reactions would be likely to increase the PS decomposition rate. In order to test any participation of chain reactions, we compared the PS decomposition activated by UV radiation (254 nm) in the presence (1 M) and absence of methanol under otherwise identical reaction conditions. The observed PS decomposition rates were found to be identical (Fig. S7). This provides clear evidence that radical chain reactions do not play a major role in PS decomposition.

3.5.4 Activation energy

As the PS activation by particulate FeS differs significantly from that by Fe^{2+} ions in solution, activation energies of the two processes under analogous conditions were compared. The oxidation of benzene to phenol was used as probe reaction for sulfate radicals. For this purpose, analogous degradation experiments were carried out at 0°C, 10°C and 25°C. Higher temperatures were avoided because of the thermal PS activation. Figure 6 shows the Arrhenius plot for the first-order rate constants obtained. The primary kinetic data are available in the SI part (Figs. S8-10). The corresponding activation energies were calculated from the slope of the linear regression lines: $E_A = (31 \pm 1) \text{ kJ mol}^{-1}$ in the presence of suspended FeS and $E_A = (72 \pm 1) \text{ kJ mol}^{-1}$ with dissolved FeSO_4 . The two values are significantly different. The lower value for the FeS-catalyzed pathway is in conformity with our hypothesis of a surface-

assisted bond cleavage (Scheme 1). For PS activation by Fe^{2+} , values previously reported in the literature are around 50 kJ mol^{-1} [5].

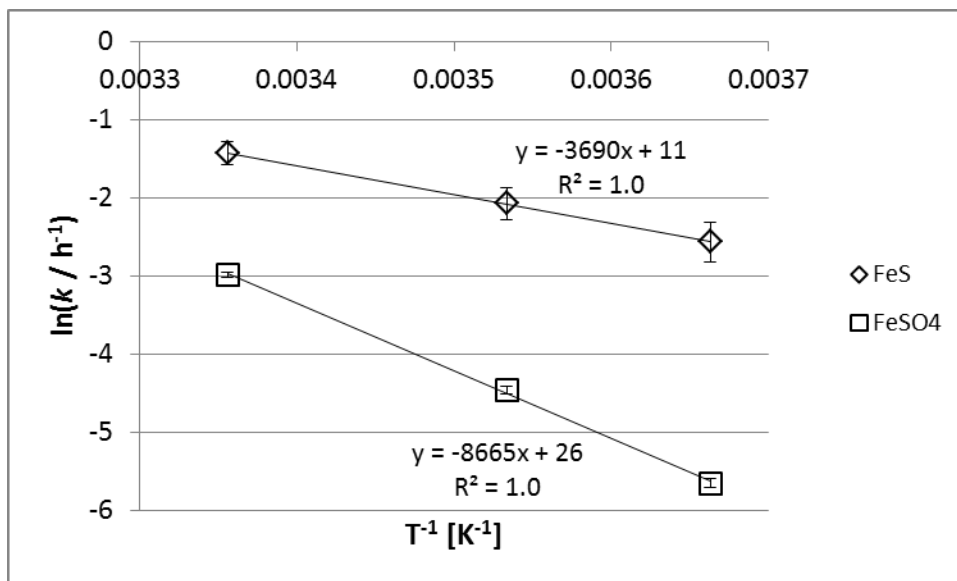
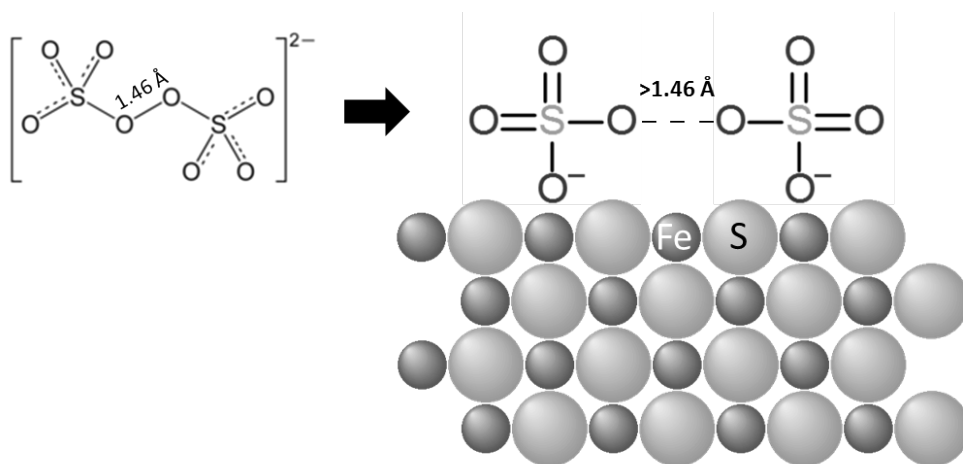


Figure 6: Arrhenius plot of the oxidation of benzene with sulfate radicals generated by the reaction of FeS and FeSO_4 with PS at 0, 10 and 25°C ($c_{\text{FeS},0} = 2.3 \text{ mM}$; $c_{\text{FeSO}_4,0} = 0.7 \text{ mM}$; $c_{\text{PS},0} = 4.2 \text{ mM}$; $c_{\text{Benzene},0} = 13 \text{ mM}$).



Scheme 1: Proposed activation mechanism of peroxydisulfate on FeS

4 Conclusions

In this study, FeS was investigated as a catalyst for PS activation. The system was used for TCE oxidation with high rates at various pH values. Favorable conditions were determined with a pH value about 5 and for both, FeS and PS concentrations of about 5 mM or slightly higher. Furthermore, the system works efficiently in the absence of dissolved oxygen. Kinetic isotope effects for H/D abstraction from cyclohexane isotopologues ($k_H/k_D = 2.2$) confirm sulfate radicals as the predominant radical species formed from PS. Mechanistic studies showed that Fe^{2+} is, in contrast to sulfide, more stable in the system. PS decomposition is inhibited in the absence of radical consumers. The stability of Fe^{2+} was further improved by the addition of small amounts of H_2O_2 . FeS was also applied in long-term experiments and showed a high life-time as activator for PS. The catalytic nature of the PS activation process was clearly proved by a turnover number of > 100 . The nature of the catalytically active species was not yet revealed. Under the chosen conditions, the FeS activation generated about 1.6 sulfate radicals from one persulfate anion. This yield is significantly different from that obtained with dissolved Fe^{2+} as activator ($0.82 \text{ mol mol}^{-1}$). It is hypothesized that FeS activates PS by a surface-assisted homolytic bond cleavage without electron transfer. Further studies are necessary for deeper insight into the reaction mechanism.

ASSOCIATED CONTENT

Supporting Information. Supplementary data and methodical comments associated with this article can be found in the online version, at <http://dx.doi.org>

Author Contributions

The manuscript was written with contributions of all authors. All authors have given approval to the final version of the manuscript.

The authors declare no competing financial interest.

ACKNOWLEDGEMENTS

This work was supported by funds of the German Federal Ministry of Education and Research (BMBF) in the frame of the project CONTASORB [grant number 03XP0090A].

REFERENCES

1. Dewil, R., et al., *New Perspectives for Advanced Oxidation Processes*. Journal of Environmental Management, 2017. **195**: p. 93-99.
2. Anipsitakis, G.P. and D.D. Dionysiou, *Degradation of Organic Contaminants in Water with Sulfate Radicals Generated by the Conjunction of Peroxymonosulfate with Cobalt*. Environmental Science & Technology, 2003. **37**(20): p. 4790-4797.
3. Armstrong, D.A., et al., *Standard Electrode Potentials involving Radicals in Aqueous Solution: Inorganic Radicals*, in *Biological Reaction Mechanisms*. 2013. p. 59-61.
4. Luo, S., et al., *Mechanistic Insight into Reactivity of Sulfate Radical with Aromatic Contaminants through Single-Electron Transfer Pathway*. Chemical Engineering Journal, 2017. **327**: p. 1056-1065.
5. Matzek, L.W. and K.E. Carter, *Activated Persulfate for Organic Chemical Degradation: A Review*. Chemosphere, 2016. **151**(Supplement C): p. 178-188.
6. Neta, P., R.E. Huie, and A.B. Ross, *Rate constants for Reactions of Inorganic Radicals in Aqueous-Solution*. Journal of Physical and Chemical Reference Data, 1988. **17**(3): p. 1027-1284.
7. Pennington, D.E. and A. Haim, *Stoichiometry and Mechanism of Chromium(2)-Peroxydisulfate Reaction*. Journal of the American Chemical Society, 1968. **90**(14): p. 3700-3704.
8. Hayon, E., A. Treinin, and J. Wilf, *Electronic-Spectra, Photochemistry, and Autooxidation Mechanism of Sulfite-Bisulfite-Pyrosulfite Systems - SO₂⁻, SO₃⁻, SO₄⁻, and SO₅⁻ Radicals*. Journal of the American Chemical Society, 1972. **94**(1): p. 47-57.
9. Liang, C., Z.-S. Wang, and C.J. Bruell, *Influence of pH on Persulfate Oxidation of TCE at Ambient Temperatures*. Chemosphere, 2007. **66**(1): p. 106-113.
10. Liang, C.J. and H.W. Su, *Identification of Sulfate and Hydroxyl Radicals in Thermally Activated Persulfate*. Industrial & Engineering Chemistry Research, 2009. **48**(11): p. 5558-5562.
11. Waldemer, R.H., et al., *Oxidation of Chlorinated Ethenes by Heat-Activated Persulfate: Kinetics and Products*. Environmental Science & Technology, 2007. **41**(3): p. 1010-1015.
12. Johnson, R.L., P.G. Tratnyek, and R.O.B. Johnson, *Persulfate Persistence under Thermal Activation Conditions*. Environmental Science & Technology, 2008. **42**(24): p. 9350-9356.

13. Guan, Y.-H., et al., *Influence of pH on the Formation of Sulfate and Hydroxyl Radicals in the UV/Peroxymonosulfate System*. Environmental Science & Technology, 2011. **45**(21): p. 9308-9314.
14. Pu, M., et al., *Synthesis of Iron-based Metal-organic framework MIL-53 as an Efficient Catalyst to Activate Persulfate for the Degradation of Orange G in Aqueous Solution*. Applied Catalysis A: General, 2018. **549**: p. 82-92.
15. Wang, J. and S. Wang, *Activation of Persulfate (PS) and Peroxymonosulfate (PMS) and Application for the Degradation of Emerging Contaminants*. Chemical Engineering Journal, 2018. **334**: p. 1502-1517.
16. Xiao, R., et al., *Activation of Peroxymonosulfate/persulfate by Nanomaterials for Sulfate Radical-based Advanced Oxidation Technologies*. Current Opinion in Chemical Engineering, 2018. **19**: p. 51-58.
17. Wacławek, S., et al., *Chemistry of Persulfates in Water and Wastewater Treatment: A Review*. Chemical Engineering Journal, 2017. **330**: p. 44-62.
18. Guan, Y.-H., et al., *Efficient Degradation of Atrazine by Magnetic Porous Copper Ferrite Catalyzed Peroxymonosulfate Oxidation via the Formation of Hydroxyl and Sulfate Radicals*. Water Research, 2013. **47**(14): p. 5431-5438.
19. Zhang, T., H. Zhu, and J.-P. Croué, *Production of Sulfate Radical from Peroxymonosulfate Induced by a Magnetically Separable CuFe₂O₄ Spinel in Water: Efficiency, Stability, and Mechanism*. Environmental Science & Technology, 2013. **47**(6): p. 2784-2791.
20. Zeng, T., et al., *Spatial Confinement of a Co₃O₄ Catalyst in Hollow Metal–Organic Frameworks as a Nanoreactor for Improved Degradation of Organic Pollutants*. Environmental Science & Technology, 2015. **49**(4): p. 2350-2357.
21. Oh, W.-D., Z. Dong, and T.-T. Lim, *Generation of Sulfate Radical through Heterogeneous Catalysis for Organic Contaminants Removal: Current Development, Challenges and Prospects*. Applied Catalysis B: Environmental, 2016. **194**(Supplement C): p. 169-201.
22. Hu, L., et al., *Inactivation of Bacteriophage MS2 with Potassium Ferrate(VI)*. Environmental Science & Technology, 2012. **46**(21): p. 12079-12087.
23. Wang, Y., et al., *Facile Synthesis of Hierarchically Structured Magnetic MnO₂/ZnFe₂O₄ Hybrid Materials and Their Performance in Heterogeneous Activation of Peroxymonosulfate*. ACS Applied Materials & Interfaces, 2014. **6**(22): p. 19914-19923.
24. Ren, Y., et al., *Sulfate Radicals induced from Peroxymonosulfate by Magnetic Ferrosphinel MFe₂O₄ (M=Co, Cu, Mn, and Zn) as Heterogeneous Catalysts in the Water*. Applied Catalysis B: Environmental, 2015. **165**(Supplement C): p. 572-578.
25. Yuan, S., P. Liao, and A.N. Alshawabkeh, *Electrolytic Manipulation of Persulfate Reactivity by Iron Electrodes for Trichloroethylene Degradation in Groundwater*. Environmental Science & Technology, 2014. **48**(1): p. 656-663.
26. Pulicharla, R., et al., *Activation of Persulfate by Homogeneous and Heterogeneous Iron Catalyst to Degrade Chlortetracycline in Aqueous Solution*. Chemosphere, 2018. **207**: p. 543-551.
27. Lin, Y.-T., C. Liang, and C.-W. Yu, *Trichloroethylene Degradation by Various Forms of Iron Activated Persulfate Oxidation with or without the Assistance of Ascorbic Acid*. Industrial & Engineering Chemistry Research, 2016. **55**(8): p. 2302-2308.
28. Wu, Y., et al., *Activation of Persulfate by Fe(III) species: Implications for 4-tert-butylphenol Degradation*. Journal of Hazardous Materials, 2017. **322**: p. 380-386.
29. Kang, J., et al., *Zero-valent iron (ZVI) Activation of Persulfate (PS) for Degradation of Para-Chloronitrobenzene in Soil*. Bulletin of Environmental Contamination and Toxicology, 2019. **103**(1): p. 140-146.

30. Ike, I.A. and M. Duke, *Synthetic Magnetite, Maghemite, and Haematite Activation of Persulphate for Orange G Degradation*. Journal of Contaminant Hydrology, 2018. **215**: p. 73-85.
31. Ike, I.A., et al., *Critical Review of the Science and Sustainability of Persulphate Advanced Oxidation Processes*. Chemical Engineering Journal, 2018. **338**: p. 651-669.
32. Anipsitakis, G.P. and D.D. Dionysiou, *Radical Generation by the Interaction of Transition Metals with Common Oxidants*. Environmental Science & Technology, 2004. **38**(13): p. 3705-3712.
33. Yuan, Y., et al., *Degradation of p-Chloroaniline by Persulfate Activated with Ferrous Sulfide Ore Particles*. Chemical Engineering Journal, 2015. **268**(Supplement C): p. 38-46.
34. Dong, H., et al., *Insights into Enhanced Removal of TCE Utilizing Sulfide-Modified Nanoscale Zero-valent iron Activated Persulfate*. Chemical Engineering Journal, 2019. **359**: p. 1046-1055.
35. Butler, E.C. and K.F. Hayes, *Factors Influencing Rates and Products in the Transformation of Trichloroethylene by Iron Sulfide and Iron Metal*. Environmental Science & Technology, 2001. **35**(19): p. 3884-3891.
36. Butler, E.C. and K.F. Hayes, *Kinetics of the Transformation of Trichloroethylene and Tetrachloroethylene by Iron Sulfide*. Environmental Science & Technology, 1999. **33**(12): p. 2021-2027.
37. Carlson, D.L., et al., *Influence of Surface Composition on the Kinetics of Alachlor Reduction by Iron Pyrite*. Environmental Science & Technology, 2003. **37**(11): p. 2394-2399.
38. Kriegmanking, M.R. and M. Reinhard, *Transformation of Carbon-Tetrachloride by Pyrite in Aqueous-Solution*. Environmental Science & Technology, 1994. **28**(4): p. 692-700.
39. Lee, W. and B. Batchelor, *Abiotic Reductive Dechlorination of Chlorinated Ethylenes by Iron-Bearing Soil Minerals. 1. Pyrite and Magnetite*. Environmental Science & Technology, 2002. **36**(23): p. 5147-5154.
40. Nefso, E.K., S.E. Burns, and C.J. McGrath, *Degradation Kinetics of TNT in the Presence of Six Mineral Surfaces and Ferrous Iron*. Journal of Hazardous Materials, 2005. **123**(1): p. 79-88.
41. Oh, S.-Y., P.C. Chiu, and D.K. Cha, *Reductive Transformation of 2,4,6-Trinitrotoluene, Hexahydro-1,3,5-trinitro-1,3,5-triazine, and Nitroglycerin by Pyrite and Magnetite*. Journal of Hazardous Materials, 2008. **158**(2): p. 652-655.
42. Patterson, R.R., S. Fendorf, and M. Fendorf, *Reduction of Hexavalent Chromium by Amorphous Iron Sulfide*. Environmental Science & Technology, 1997. **31**(7): p. 2039-2044.
43. Weerasooriya, R. and B. Dharmasena, *Pyrite-Assisted Degradation of Trichloroethene (TCE)*. Chemosphere, 2001. **42**(4): p. 389-396.
44. Zouboulis, A.I., K.A. Kydros, and K.A. Matis, *Removal of Hexavalent Chromium Anions from Solutions by Pyrite Fines*. Water Research, 1995. **29**(7): p. 1755-1760.
45. Oh, S.-Y., et al., *Degradation of 2,4-Dinitrotoluene by Persulfate Activated with Iron Sulfides*. Chemical Engineering Journal, 2011. **172**(2): p. 641-646.
46. Fan, J., et al., *Mackinawite (FeS) Activation of Persulfate for the Degradation of p-Chloroaniline: Surface Reaction Mechanism and Sulfur-Mediated Cycling of Iron Species*. Chemical Engineering Journal, 2018. **333**: p. 657-664.
47. Chen, H., et al., *Degradation of 2,4-Dichlorophenoxyacetic Acid in Water by Persulfate Activated with FeS (Mackinawite)*. Chemical Engineering Journal, 2017. **313**: p. 498-507.
48. Liang, C., et al., *A rapid Spectrophotometric Determination of Persulfate Anion in ISCO*. Chemosphere, 2008. **73**(9): p. 1540-1543.
49. Liang, C., et al., *Persulfate Oxidation for In Situ Remediation of TCE. I. Activated by Ferrous Ion with and without a Persulfate-Thiosulfate Redox Couple*. Chemosphere, 2004. **55**(9): p. 1213-1223.

50. Liang, C. and C.J. Bruell, *Thermally Activated Persulfate Oxidation of Trichloroethylene: Experimental Investigation of Reaction Orders*. Industrial & Engineering Chemistry Research, 2008. **47**(9): p. 2912-2918.
51. Kopinke, F.-D. and A. Georgi, *What Controls Selectivity of Hydroxyl Radicals in Aqueous Solution? Indications for a Cage Effect*. The Journal of Physical Chemistry A, 2017. **121**(41): p. 7947-7955.
52. Lobachev, V.L., et al., *Kinetics and Anomalous Temperature Dependence of the Kinetic Isotope Effect of Reactions of Cycloalkanes C₅H₁₀, C₆H₁₂ and C₆D₁₂ with OH Radicals in Aqueous Solutions*. Theoretical and Experimental Chemistry, 2008. **44**(1): p. 37-41.
53. Rastogi, A., S.R. Al-Abed, and D.D. Dionysiou, *Sulfate Radical-Based Ferrous–Peroxymonosulfate Oxidative System for PCBs Degradation in Aqueous and Sediment Systems*. Applied Catalysis B: Environmental, 2009. **85**(3): p. 171-179.
54. Chen, K.F., et al., *Methyl tert-butyl ether (MTBE) Degradation by Ferrous Ion-Activated Persulfate Oxidation: Feasibility and Kinetics Studies*. Water Environment Research, 2009. **81**(7): p. 687-694.
55. Yen, C.-H., et al., *Application of Persulfate to Remediate Petroleum Hydrocarbon-Contaminated Soil: Feasibility and Comparison with Common Oxidants*. Journal of Hazardous Materials, 2011. **186**(2): p. 2097-2102.
56. Ruan, X., et al., *Trichloroethylene Degradation by Persulphate with Magnetite as a Heterogeneous Activator in Aqueous Solution*. Environmental Technology, 2015. **36**(11): p. 1389-1397.
57. Ahmad, M., et al., *Oxidative and Reductive Pathways in Iron-Ethylenediaminetetraacetic Acid-Activated Persulfate Systems*. Journal of Environmental Engineering, 2012. **138**(4): p. 411-418.
58. Wu, X., et al., *Degradation of Trichloroethylene in Aqueous Solution by Persulfate Activated with Citric Acid Chelated Ferrous Ion*. Chemical Engineering Journal, 2014. **255**: p. 585-592.
59. Chiriță, P., *Evaluation and Modeling of the Surface Characteristics of Troilite (FeS)*. Applied Surface Science, 2019. **480**: p. 281-287.
60. Kolthoff, I.M. and I.K. Miller, *The Chemistry of Persulfate.1. The Kinetics and Mechanism of the Decomposition of the Persulfate Ion in Aqueous Medium*. Journal of the American Chemical Society, 1951. **73**(7): p. 3055-3059.
61. Zhang, Y.Q., et al., *Efficient Pyrite Activating Persulfate Process for Degradation of p-Chloroaniline in Aqueous Systems: A Mechanistic Study*. Chemical Engineering Journal, 2017. **308**: p. 1112-1119.
62. Xia, D., et al., *Activation of Persulfates by Natural Magnetic Pyrrhotite for Water Disinfection: Efficiency, Mechanisms, and Stability*. Water Research, 2017. **112**: p. 236-247.
63. Moses, C.O., et al., *Aqueous Pyrite Oxidation by Dissolved Oxygen and by Ferric Iron*. Geochimica et Cosmochimica Acta, 1987. **51**(6): p. 1561-1571.
64. Kwan, W.P. and B.M. Voelker, *Decomposition of Hydrogen Peroxide and Organic Compounds in the Presence of Dissolved Iron and Ferrihydrite*. Environmental Science & Technology, 2002. **36**(7): p. 1467-1476.
65. Tsitonaki, A., et al., *In Situ Chemical Oxidation of Contaminated Soil and Groundwater Using Persulfate: A Review*. Critical Reviews in Environmental Science and Technology, 2010. **40**(1): p. 55-91.
66. Baumgartner, J. and D. Faivre, *Iron Solubility, Colloids and their Impact on Iron (oxyhydr)oxide Formation from Solution*. Earth-Science Reviews, 2015. **150**: p. 520-530.
67. Morgan, B. and O. Lahav, *The Effect of pH on the Kinetics of Spontaneous Fe(II) Oxidation by O₂ in Aqueous Solution – Basic Principles and a Simple Heuristic Description*. Chemosphere, 2007. **68**(11): p. 2080-2084.

68. Georgi, A., et al., *Accelerated Catalytic Fenton Reaction with Traces of Iron: An Fe–Pd-Multicatalysis Approach*. *Environmental Science & Technology*, 2016. **50**(11): p. 5882-5891.
69. Ball, D.L., M.M. Crutchfield, and J.O. Edwards, *The Mechanism of the Oxidation of 2-Propanol by Peroxydisulfate Ion*. *The Journal of Organic Chemistry*, 1960. **25**(9): p. 1599-1611.
70. Dominguez, C.M., et al., *Methanol-enhanced Degradation of Carbon Tetrachloride by Alkaline Activation of Persulfate: Kinetic Model*. *Science of The Total Environment*, 2019. **666**: p. 631-640.
71. Chandra, A.P. and A.R. Gerson, *Pyrite (FeS₂) Oxidation: A Sub-Micron Synchrotron Investigation of the Initial Steps*. *Geochimica et Cosmochimica Acta*, 2011. **75**(20): p. 6239-6254.
72. Bartlett, P.D. and J.D. Cotman, *The Kinetics of the Decomposition of Potassium Persulfate in Aqueous Solutions of Methanol*. *Journal of the American Chemical Society*, 1949. **71**(4): p. 1419-1422.